Numerical Simulation of Flow and Heat Transfer of Nanofluid around a Heated Square Cylinder

L. Bouazizi[1,2†] and S. Turki[1,3]

[1]*Unit of Computational Fluid Dynamics and Transfer Phenomena, National Engineering School of Sfax, Tunisia*
[2] *Department of Mechanical, National Engineering School of Sfax, BP W-3038, 1173 Sfax, Tunisia*
[3] *Faculty of Sciences of Sfax, Department of Physics, BP 1171, 3000 Sfax-University of Sfax, Tunisia*

†*Corresponding Author Email:lot.bouazizi@yahoo.fr*

ABSTRACT

A numerical investigation was conducted to study the forced and mixed convection of nanofluid in a horizontal channel with a built-in-heated square cylinder. The nanofluid considered in this study is composed of metal nanoparticles(Cu) suspended in water (base fluid). The governing equations are solved using the finite volume method based SIMPLER algorithm. Different Reynolds numbers and volume fractions of nanoparticles ranging respectively from $Re = 85$ to 200 and from $\varphi = 0\%$ to 12%, have been considered. The effect of the nanoparticles volume fraction on the critical Reynolds number value defining the transition between two flow regimes (stationary and periodic)as well as on the overall flow coefficients is firstly studied. In the thermal study, we have established correlations to evaluate the heat flux transferred from the obstacle to the flow for different nanoparticles volume fractions. Results show a marked improvement in heat transfer compared to the base fluid. This improvement is more pronounced for higher Richardson numbers and higher nanoparticles volume fractions.

Keywords: Laminar channel flow; Nanofluid; Forced and Mixed convection; Lift and drag coefficients; Strouhal number; heat transfer.

NOMENCLATURE

Cd	drag coefficient	u, v	velocity components nondimensionalized by u_0
C_p	specific heat of the fluid	V	velocity vector nondimensionalized by u_0
$\langle Cd \rangle$	time-averaged drag coefficient	x, y	cartesien coordinates nondimensionalized by h
Cl	lift coefficient	x_u	distance from body to inlet
f	dominant frequency	x_d	distance from body to outlet
h	side length of the square cylinder		
H	channel width		
k	thermal conductivity	α	thermal diffusivity
L	length of the channel	β	coefficient of thermal expansion
$\dot{m}$	flow rate	ϕ	transport quantity
$\langle \dot{m} \rangle$	time-averaged flow rate	φ	nanoparticles volume fraction
$\overline{Nu}$	space-averaged Nusselt number	ν	kinematic viscosity
$\langle \overline{Nu} \rangle$	time and space-average Nusselt number	μ	dynamic viscosity
$\langle \overline{Nu_t} \rangle$	global time and space-average Nusselt number	θ	dimensionless temperature
P	dimensionless pressure	ρ	density
p	pressure nondimensionalized by $\rho u_0{}^2$	τ	time dimensionalized by
Pr	Prandtl number		
Re	Reynolds number	**Subscripts**	
Re_c	critical Reynolds number corresponding to the transition from steady to periodic flow	nf	Nanofluid

	regimes		
Ri	Richardson number	f	Fluid
St	Strouhal Number	s	Solid
T	dimensional temperature	c	cold
t	time nondimensionalized by	h	hot
u_{av}	mean channel inlet velocity		
u_0	maximum of u-component at the channel inlet		

1. INTRODUCTION

It is well known that the flow of fluids past bluff bodies has been the subject of several researches, both experimental and theoretical. The motivation behind these studies was to understand the physical phenomenon that occurs behind the bluff body and find practical applications in industrial processes, such as aerodynamics, flow dividers in polymer processing applications, heat exchanger systems, cooling of electronic components, etc. Since the pioneer work of Davis and Moore (1982), a series of papers have dealt with flow of pure fluid past square cylinders and extensive reviews of the pertinent studies are available in the literature (Kelkar *et al*. 1992 ; Sohankar *et al*. 1998 ; Breuer *et al*. 2000 ; Darekar and Sherwin 2001 ; Turki *et al*. 2003a, 2003b ; Bouaziz *et al*. 2010 and Liu 2010) where a wealth of information on the effects of physical parameters which play a dominant role on the global flow coefficients including drag, lift and wake characteristics, vortex shedding frequency and their effect on the rate of heat transfer has been accumulated.

While there has been an enormous amount of efforts put in flow and heat transfer of pure fluids past a bluff body under appropriate conditions, very few studies have been undertaken in this area using nanofluids. This new class of fluids, composed of metal nanoparticles suspended in a base fluid, has recently appeared, due to their anomalous thermal conductivity enhancement and many studies (Daungthongsuk *et al*. (2007), Kakaç *et al*. (2009), Saidur *et al*. (2011), Fazeli *et al*. (2012), Hashemi *et al*. (2012), Zirakzadeh *et al*. (2012), Mahian *et al*. (2013), Sohel *et al*. (2013), Rashad (2013), Safaei *et al*. (2014), Sarafraz (2014), Nayak *et al*. (2015), …) have been undertaken in the area of flow and heat transfer of nanofluids, showing that these new fluids have a remarkable power of heat exchange compared to conventional liquid. This enhanced thermal behavior of nanofluids could provide a basis for an enormous innovation for heat transfer intensification, which is a major importance to a number of industrial sectors including transportation, power generation, heating, cooling, ventilation and air-conditioning, etc.

Concerning the flow of nanofluids around a bluff body, we cite for example the work of Valipour *et al*. (2011) who studied the effect of the nanoparticles volume fraction on the flow pattern and heat transfer characteristics around a circular cylinder. They showed that the length of the recirculation zone increases with the nanoparticles volume fraction. In addition, the local and the averaged Nusselt numbers were strengthened by the addition of nanoparticles to the base fluid. Sarkar *et al*. (2012) studied the vortex structure distributions and the mixed convective heat transfer of nanofluid past a confined circular cylinder. Their results show that the Strouhal number St increases by increasing the nanoparticles volume fraction and this increment in St leads to reduction in vortex shedding. In mixed convection, correlations of averaged Nusselt number in terms of volume fraction φ and Reynolds number Re have been obtained for different Richardson number. Sarkar *et al*. (2013) have simulated also the flow and heat transfer of nanofluids past a square cylinder in vertically upward flow. They examined the effect of the nanoparticles volume fraction on the overall flow coefficients such us the Strouhal number (St), the drag coefficient (Cd) and the lift coefficient (Cl). In addition, they showed the important effect of nanoparticles on heat transfer for Cu-water nanofluid compared to Al_2O_3-water nanofluid. A numerical study was conducted by Valipoor *et al*. (2014) to simulate the steady laminar forced convection flow and heat transfer of Al_2O_3-water nanofluid around a square cylinder. They reported that the Nusselt number, drag coefficient, recirculation length and pressure coefficient increase as the solid volume fraction increases.

The present research work was carried out to contribute to the existing knowledge of flow and its related heat transfer around a bluff body using nanofluid. It is a numerical investigation of forced and mixed convection of Cu-water nanofluid in a horizontal channel with a built-in-heated square cylinder. The study is particularly focused on the effect of nanoparticles volume fraction on the dynamic behavior of the flow and the heat transfer characteristics transferred from the square cylinder.

2. GOVERNING EQUATIONS

The flow geometry and coordinate system along are shown in Fig. 1. The conservation equations describing the flow are the time-dependent, two-dimensional Navier-Stokes and energy equations of incompressible nanofluid. The base fluid (water) and the nanoparticles (Cu) are assumed to be in thermal equilibrium and all the physical properties of nanofluid (Table 1) are assumed to be constant. Using the Boussinesq approximation, the

dimensionless of the continuity, momentum and thermal energy equations governing the laminar flow can be written in the following conservative form:

$$div(V) = 0 \tag{1}$$

$$\frac{\partial u}{\partial \tau} + div(J_u) = -\frac{\rho_f}{\rho_{nf}}\frac{\partial P}{\partial x},$$

$$J_u = uV - \frac{1}{Re}\frac{\mu_{nf}}{\mu_f}\frac{\rho_f}{\rho_{nf}}grad(u) \tag{2}$$

$$\frac{\partial v}{\partial \tau} + div(J_v) = -\frac{\rho_f}{\rho_{nf}}\frac{\partial P}{\partial y} + \frac{\varphi\rho_s\beta_s+(1-\varphi)\rho_f\beta_f}{\rho_{nf}\beta_f}Ri\theta,$$

$$J_v = vV - \frac{1}{Re}\frac{\mu_{nf}}{\mu_f}\frac{\rho_f}{\rho_{nf}}grad(v) \tag{3}$$

$$\frac{\partial \theta}{\partial \tau} + div(J_\theta) = 0,$$

$$J_\theta = \theta V - \frac{1}{Re.Pr}\frac{\alpha_{nf}}{\alpha_f}grad(\theta) \tag{4}$$

where ρ, β, μ, α and φ are the density, the coefficient of thermal expansion, the dynamic viscosity, the thermal diffusivity and the nanoparticles volume fraction respectively, taking into account subscripts *f* for fluid, *s* for solid and *nf* for nanofluid.
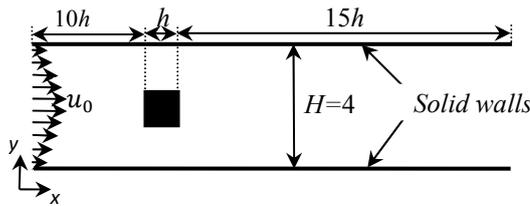
Fig. 1. Configuration definition.

Table 1 Thermophysical properties

Property	Fluid phase (Water)	Cu
Cp (J/kg K)	4179	385
ρ (kg/m³)	997.1	8933
k (W/m K)	0.613	400
$\alpha \times 10^7$ (m²/s)	1.47	1163.1

In the above equations, the space coordinates, velocities, time and pressure are normalized with the width of the square cylinder h, the maximum velocity of the channel inlet u_0, the characteristic time h/u_0 and the characteristic pressure $\rho_f u_0^2$ respectively. The dimensionless variable θ was defined as: $\theta = (T - T_c)/(T_h - T_c)$ where T_h and T_c are hot and cold temperatures respectively.

In equations (2)-(4), the viscosity of the nanofluid is given by Brinkman (1952) as follow:

$$\mu_{nf} = \frac{\mu_f}{(1-\varphi)^{2.5}} \tag{5}$$

The thermal diffusivity of the nanofluid is defined as follow:

$$\propto_{nf} = \frac{k_{nf}}{(\rho c_p)_{nf}} \tag{6}$$

where the conductivity of nanofluid k_{nf} is expressed as (Khanafer *et al*. 2003):

$$\frac{k_{nf}}{k_f} = \frac{k_s+2k_f-2\varphi(k_f-k_s)}{k_s+2k_f+\varphi(k_f-k_s)} \tag{7}$$

The effective density ρ_{nf} and the heat capacitance $(\rho c_p)_{nf}$ of the nanofluid are expressed as (Xuan *et al*. 2003):

$$\rho_{nf} = (1 - \varphi)\rho_f + \varphi\rho_s \tag{8}$$

$$(\rho c_p)_{nf} = (1 - \varphi)(\rho c_p)_f + \varphi \tag{9}$$

The Reynolds number *Re*, Richardson number *Ri* and Prandtl number *Pr* are defined as follows:

$$Re = \frac{\rho_f u_0 h}{\mu_f}, i = \frac{Gr}{Re^2}, Pr = \frac{\nu_f}{\alpha_f} \tag{10}$$

where ν_f is the kinematic viscosity of the base fluid and *Gr* is the Grashof number defined as:

$$Gr = \frac{g\beta_f h^3(T_h-T_c)}{\nu_f^2}.$$

No-slip boundary conditions for velocities on all solid walls are used. The upper and the lower channel walls are specified as adiabatic. At the channel inlet, a normal component of velocity is assumed to be zero and a fully developed parabolic profile for the axial velocity, expressed by $u = \frac{y}{4}(4 - y)$, is deployed. At the channel exit, the convective boundary condition (CBC), given by $\frac{\partial \emptyset}{\partial t} + u_{av}\frac{\partial \emptyset}{\partial x} = 0$, is used where the variable ϕ is the dependent variable (u, v, θ). It is noted here that, as mentioned by Sohankar *et al*. (1998) and Abbassi *et al*. (2002), the CBC reduces the number of iterations per time step and requires a shorter upstream computational domain as compared to the case of the Neumann boundary condition. The square cylinder is assumed to be isothermally heated at T_h, exchanging heat to the cold fluid flowing around it, which is at a uniform temperature T_c at the channel inlet.

The instantaneous values of the drag and lift coefficients on the cylinder were calculated at each time step. They are defined as:

$$Cd = \frac{F_D}{\frac{1}{2}\rho u_0^2 h} \tag{11}$$

$$Cl = \frac{F_L}{\frac{1}{2}\rho u_0^2 h} \tag{12}$$

where F_D and F_L are the drag and lift forces exerted by the fluid on the cylinder, respectively. These forces are calculated by integration the viscous shear forces and pressure over the surface of the cylinder.

The thermal heat flux transferred from each face of the square cylinder to the flow is characterized by the space-averaged Nusselt number, and it is

Table 2 Values of St, $\langle CD \rangle$ and $[\max\,(CL) - \min\,(CL)]$ obtained with different grids ($Re = 150$ and $\varphi = 0$)

Grid	$G1: 101x41$ $0.05 \leq \Delta x \leq 0.6$ $\Delta y = 0.1$	$G2: 249x93$ $0.01 \leq \Delta x \leq 0.4$ $0.01 \leq \Delta y \leq 0.05$	$G3: 312x169$ $0.005 \leq \Delta x \leq 0.2$ $0.005 \leq \Delta y \leq 0.025$
St	0.2176	0.1924	0.1892
$\langle CD \rangle$	2.056	1.59	1.565
$[\max(CL) - \min(CL)]$	0.2512	0.2168	0.2136

defined as follow:

$$\overline{Nu} =$$
$$\begin{cases} \int_0^1 (-\frac{k_{nf}}{k_f}\frac{\partial\theta}{\partial x})_{wall}\,dy : on\ the\ transverse \\ \qquad surfaces\ of\ the\ cylinder \\ \\ \int_0^1 (-\frac{k_{nf}}{k_f}\frac{\partial\theta}{\partial y})_{wall}\,dx: on\ the\ toporbottom \\ \qquad surfaces\ of\ the\ cylinder \end{cases} \quad (13)$$

The time and space-averaged Nusselt number on each face of the square cylinder is evaluated as:

$$\langle \overline{Nu} \rangle = \frac{1}{\tau_2-\tau_1}\int_{\tau_1}^{\tau_2} \overline{Nu}\,dt \quad (14)$$

where the time interval $(\tau_2 - \tau_1)$ is large compared to the period of oscillations and usually chosen as an integer multiple of period. The global time and space-averaged Nusselt number is written as:

$$\langle \overline{Nu_t} \rangle = \sum_{\text{all faces}}\langle \overline{Nu} \rangle/4 \quad (15)$$

3. NUMERICAL METHOD OF SOLUTION

The combined continuity, momentum and energy equations are solved using a finite volume method of Patankar (1980), in which the control volume cells for velocity components are staggered with respect to the main control volume cells. This use of a staggered grid prevents the occurrence of checkerboard pressure fields. The convection terms in equations (2-4) were discretized using hybrid scheme, while the diffusion terms were discretized using second order central scheme. The SIMPLER algorithm was applied to solve the pressure-velocity coupling in conjunction with an alternating direction implicit scheme to perform the time evolution. The detailed information of the numerical procedure is given by Turki *et al.* (1990a) and more details about the validity of the computational code used in this work are available in Bouazizi *et al.* (2013).

4. RESULTS AND DISCUSSION

4.1. Grid Independence Study

To check the effect of grid spacing, computations were performed for three different meshes with $G1: 101 \times 41$, $G2: 249 \times 93$ and $G3: 312 \times 169$ non uniform grids at $Re = 150$ and $\varphi = 0$ (pure water). In the region which extends 0.5 units from each solid wall, the grid has been made finer by using an exponential stretch described in detail in the work of Turki *et al.* (1990a). Otherwise, we have used an arithmetic function. This technique is used to evaluate the strong variation of all variables near the walls. Results of the Strouhal number St, the time-avraged drag coefficient $\langle Cd \rangle$ and the amplitude of the CL oscillations values obtained with these different grids are reported in Table 2. As it can be seen, results obtained with $G2$ and $G3$ grid systems agree with each other. Indeed, the St, $\langle Cd \rangle$ and the amplitude of the CL oscillations values undergo a variation of 11.6%, 22.7% and 13.7% when we pass from $G1\ to\ G2$ grid systems, respectively, and 1.7%, 1.6% and 1.5% when we pass from $G2\ to\ G3$ grid systems, respectively. Finer grid spacing may give a more accurate solution; however, refinement of the accuracy of computation will be small after increasing the number of grid points beyond a certain level. At the same time, computational cost becomes greater. In the present computation, the $G2$ grid system was adopted based on the trade-off between accuracy and cost of the computation.

4.2. Forced Convection ($Ri = 0$)

Figure 2 shows the variation of the critical Reynolds number Re_c, defining the transition from steady to periodic flow regimes, versus the nanoparticles volume fraction (φ). As mentioned by Turki *et al.* (2003b), the steady flow regime, corresponding to $Re < Re_c$, is characterized by the appearance of two counter-rotating vortices behind the square cylinder while the periodic flow regime, corresponding to $Re \geq Re_c$, is characterized by an alternate shedding of a single vortex pair from the rear face of the square cylinder over one periodic cycle giving rise to the formation of the Von Karman wake. As reported in Fig. 2, it is clear that the presence of nanoparticles in the pure fluid (water) has a remarkable effect on the value of the critical Reynolds number, especially at low nanoparticles volume fractions. Re_c decreases rapidly by increasing φ, reaches a local minimum at $\varphi = 6\%$ and then it increases slowly as φ increases. Indeed, by increasing φ from 0% to 6%, the critical Reynolds number undergoes a reduction of the order of 29%, while a slight increase in Re_c of about 17% is observed when φ increases from 6% to 12%. The curve $Re_c = f(\varphi)$ separates the diagram presented in Fig. 2 into two areas allowing to define the behavior of the flow downstream the square cylinder for a given couple (φ, Re).
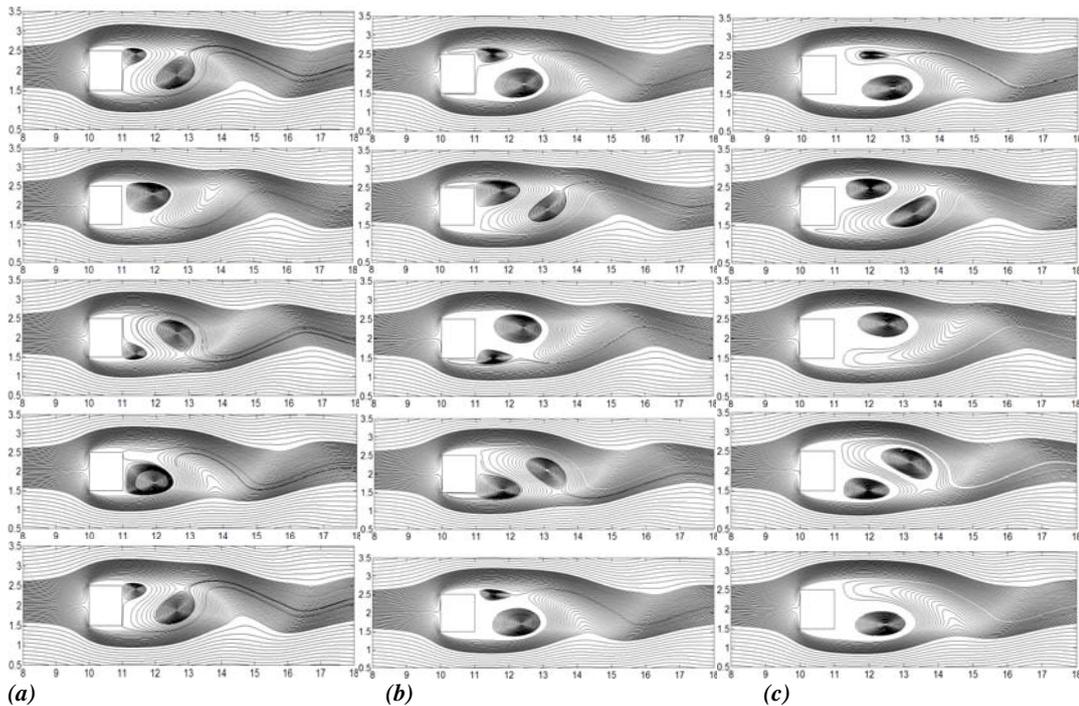
Fig. 3. Streamlines crossing the square cylinder in the channel at $Re = 150$ **(a):** $\varphi = 0$% **(b):**$\varphi = 6$% **(c):** $\varphi = 12$%.
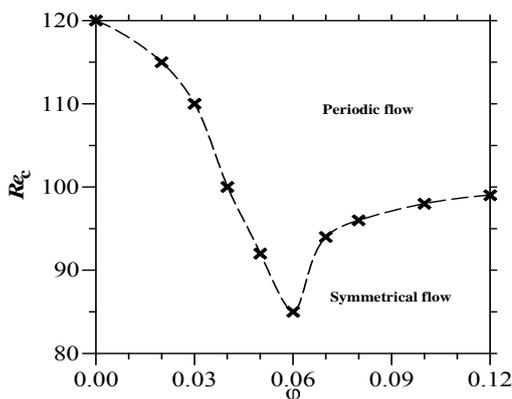
Fig. 2. Variation of the critical Reynolds number vsnanoparticles volume fraction.

Figure 3(a) shows the instantaneous streamlines around the square cylinder at equal interval times during one period of vortex shedding for pure fluid ($\varphi = 0$%). At the same time, we have presented in Figs 3(b) and 3(c) the instantaneous streamlines around the square cylinder for $\varphi = 6$% and $\varphi = 12$% respectively. Close observation of Fig.3 reveals that the vortices which shed from the square cylinder move slowly downstream the square cylinder as the volume fraction of nanoparticles increases. This can be explained by the increase of the dynamic viscosity of the nanofluid with the increase of φ (see equation 5) and hence the friction forces on the square cylinder walls increase. These forces tend to oppose to the detachment of vortices from the cylinder delaying therefore their diffusion downstream the square cylinder. The presence of nanoparticles seems to have influenced the vortex shedding from the square cylinder, resulting therefore in the modification of the Strouhal

number, characterizing the frequency of vortex shedding. Indeed, as shown in Fig.4 where we have presented the effect of the nanoparticles volume fraction on the variation of St with Re, the Strouhal number increases very slowly by increasing the Reynolds number, reaches a local maximum at $Re = 140$ and 120 for $\varphi = 0$% and $\varphi = 6$% respectively and then decreases. For $\varphi = 12$%, and contrarily to what was observed for $\varphi = 0$% and $\varphi = 6$%, the Strouhal number decreases progressively over the entire Re range. Close observation of Fig.4 reveals that the Strouhal number was influenced by the nanoparticles volume fraction, especially for higher Reynolds number. For example, at $Re = 200$, the St value undergoes a reduction of 9.3% and 7.5% when φ increases from 0% to 6% and from 6% to 12%, respectively. We note that the reduction in the Strouhal number implies a delay of vortex shedding

The variation of the lift coefficient Cl, plotted by $[max(Cl) - min(Cl)]$ versus Re is illustrated in Fig. 5 for different nanoparticles volume fractions. For all volume fraction φ considered in this study, these variations have a similar trend. The amplitude of Cl oscillations increases smoothly by increasing Re, but, as it can be seen, the $[max(Cl) - min(Cl)]$ obtained at $\varphi = 12$%, shows a very strong increase at higher Reynolds number compared to those obtained for $\varphi = 0$% and $\varphi = 6$%. For example, the amplitudes of the Cl oscillations, obtained at $\varphi = 12$%, are about 2 and 2.45 times as much as the ones obtained at $\varphi = 0$% and $\varphi = 6$% respectively when Re reaches 200. Departing from these significant results, it seems that the increase in the concentration of nanoparticles makes the square cylinder in unstable

posture to the flow for high Reynolds numbers.
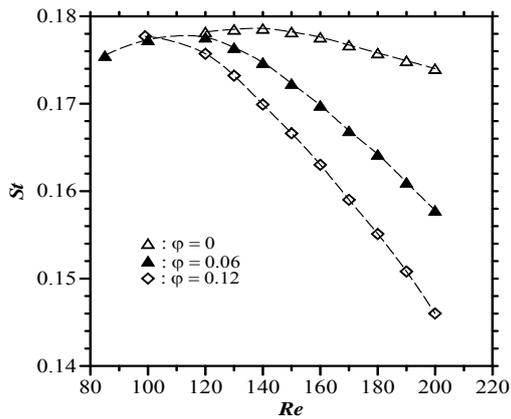
Fig. 4. Effect of the volume fraction of nanoparticles on variation in St with Re.
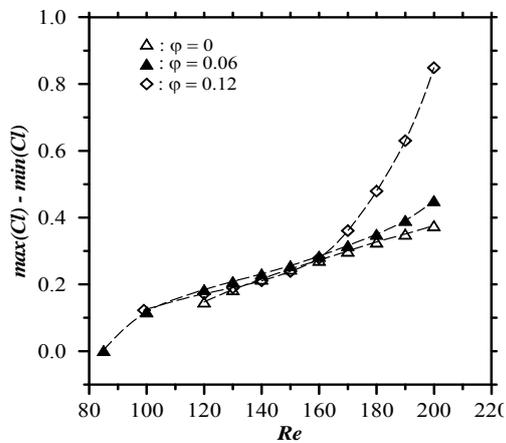
Fig. 5. Effect of the volume fraction of nanoparticles on variation in lift coefficient.

Figure 6 depicts the variation of the time-averaged drag coefficient $\langle Cd \rangle$ with Reynolds number for different nanoparticles volume fraction. As it can be seen, a local minimum on $\langle Cd \rangle$ curve occurs at $Re = 130$ and 100 for $\varphi = 6\%$ and 12%, respectively. Whereas, the drag variation decreases progressively with increasing Re for $\varphi = 0$. Close observation of Fig. 6 reveals that the time-averaged drag coefficient is influenced by the presence of nanoparticles, especially for $\varphi = 12\%$ where a digressive increase is observed on the $\langle Cd \rangle$ value when Re increases. For example, when Re reaches 200, the $\langle Cd \rangle$ values, obtained at $\varphi = 6\%$ and $\varphi = 12\%$ have undergo an increase of 3.6% and 9.2% compared to the value obtained at $\varphi = 0$. Based on these results, it seems that, by increasing the concentration of nanoparticles, the drag forces exerted by the fluid on the square cylinder become more significant than that in pure fluid ($\varphi = 0$), causing therefore an abrupt increase in $\langle Cd \rangle$ when Re increases. As already mentioned, this is related to the increment of the dynamic viscosity of the nanofluid when φ increases.
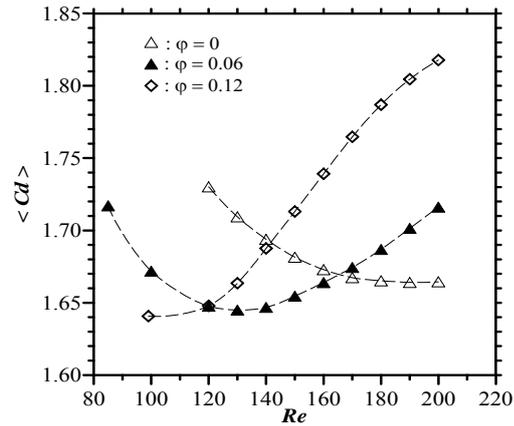
Fig. 6. Effect of the volume fraction of nanoparticles on variation in time-averaged drag coefficient.

The effect of nanoparticles on the heat transfer is examined for Re ranging from 85 to 200 and $\varphi = 0\%, 6\%$ and 12%. Three snapshots of temperature contours around the square cylinder are displayed in Fig. 7 for these different nanoparticles volume fractions. These snapshots, obtained at $Re = 150$, correspond to an arbitrary instant when the flow is well established. As it can be seen, a high temperature gradient is visible from the contours especially near the front face which has the thinner thermal boundary layers, then the highest heat transfer rates occurs near this face. In addition, the thermal boundary layer around the solid walls of the square cylinder was found thinner when φ increases. As a consequence, the heat transfer rate from the heated square cylinder becomes higher when the volume fraction of nanoparticles increases. Figure 8 confirms this result where we have plotted the global time averaged Nusselt number $\langle \overline{Nu_t} \rangle$ over the heat transfer surface of the square cylinder against the Reynolds number for different nanoparticles volume fractions. As it can be seen, for each value of φ, the heat transfer rate increases monotonously when Re increases and this enhancement was found more important for higher value of φ. For example, an increase of 19% and 42% in heat transfer is observed at $Re = 200$ when we pass from $\varphi = 0\%$ to 6% and from $\varphi = 0\%$ to 12% respectively. Referring back to Fig. 8 again, changes in slope for $\langle \overline{Nu_t} \rangle$-curves are observed around $Re = 150$ and 140 for $\varphi = 6\%$ and $\varphi=12\%$, respectively. As mentioned by Turki *et al*. (1990b), this change characterizes flow transitions from asymptotic to boundary layer regime. For each nanoparticles volume fraction considered in this section, and in the range of Reynolds number where the slopes of the curves of Ln ($\langle \overline{Nu_t} \rangle$) versus Ln*(Re)* are almost constant, a least-square method has been used for all computed data of $\langle \overline{Nu_t} \rangle$ to get a linear fit on a plot of Ln($\langle \overline{Nu_t} \rangle$) against Ln *(Re)*. Hence, it is possible to correlate the global time-averaged Nusselt number $\langle \overline{Nu_t} \rangle$ according to $\langle \overline{Nu_t} \rangle = c\mathrm{Re}^d$, the following expression may be derived.

For $\varphi = 0\%$:
$c = 1.264$; $d = 0.301$ $120 \leq Re \leq 200$

$$(16\text{-}1)$$

For $\varphi = 6\%$
$\begin{cases} c = 1.069 \ ; \ d = 0.347 & 85 \leq Re \leq 150 \\ c = 0.184 \ ; \ d = 0.696 & 150 \leq Re \leq 200 \end{cases}$

$$(16\text{-}2)$$

For $\varphi = 12\%$
$\begin{cases} c = 0.412 \ ; d = 0.563 & 100 \leq Re \leq 140 \\ c = 0.125 \ ; d = 0.804 & 140 \leq Re \leq 200 \end{cases}$

$$(16\text{-}3)$$

(c)

(b)

(a)
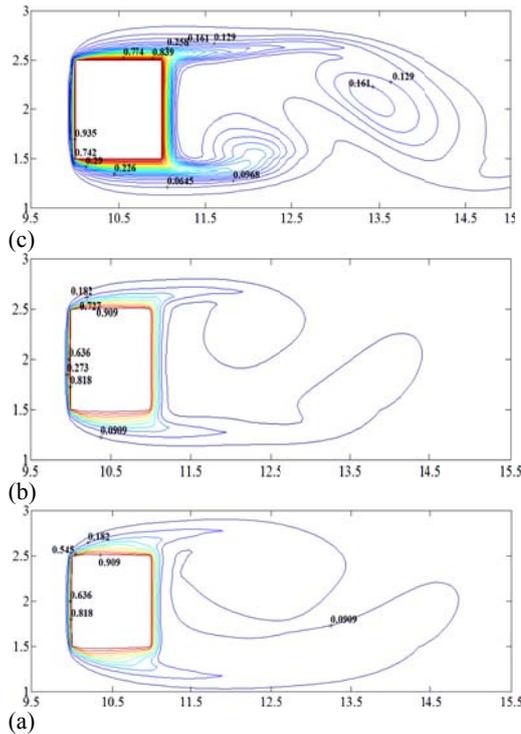
Fig. 7. Temperature contours surrounding the square cylinder at Re = 150 (a): $\varphi = 0\%$, (b): $\varphi = 6\%$, (c): $\varphi = 12\%$.
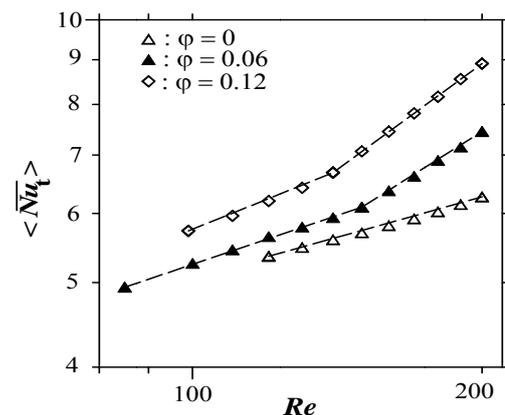
Fig. 8. Variation of the global time averaged Nusselt number versus Re for different φ.

4.3.   Mixed Convection

In this section we examine the effect of the nanoparticles volume fraction on the flow pattern and the heat transfer characteristics for Richardson number Ri up to 4.5 at a fixed Reynolds number

$Re = 150$ and Prandtl number $Pr = 6.2$. It should be noted that the flow was found in unstable state when Ri exceeds the value of 4.5. Figure 9 shows the streamlines crossing the square cylinder in the channel for different Richardson numbers. When the Richardson number increases and in the absence of the nanoparticles ($\varphi = 0\%$), the velocity of particle fluids behind the rear face of the cylinder increases and moves toward the upper channel wall. The mass conservation dictates an increased fluid velocity below the square cylinder. As a consequence, when the flow approaches the front face of the cylinder, most of the fluids are flowing below the bottom side of the cylinder. For $\varphi = 12\%$, the effect of the buoyancy forces is found less important when Ri increases. This can be explained by the thermopheresis forces effect. Indeed, when the nanoparticles approaching the obstacle, they heat up and quickly move away towards the cold zone of nanofluid. These hot nanoparticles collide with cold particles and under the thermopheresis forces effect, they move toward the horizontal walls of the channel, causing therefore the migration of the nanofluid through the sections below and above the cylinder.

Figure 10 depicts the variation of the time-averaged flow rates of the nanofluid through the sections between the square cylinder and the channel walls versus Richardson numbers for different nanoparticles volume fractions. As it can be seen, for each nanoparticles volume fraction considered in this study, the computations show that the buoyancy effect becomes appreciable and modifies the global structure of the flow around the body when Ri exceeds 0.8. It should be noted, as mentioned by Abbassi *et al*. (2002), that in pure forced convection the flow rates through the sections above and below the cylinder fluctuate in opposition of phase about the half average value of the flow rate at the channel inlet. In addition, the frequency of fluctuation is the same to that of vortex shedding. When the Richardson number exceeds 0.8, the two flow rates usually fluctuate in opposition of phase but each other around its average value which is found to be more important below the square cylinder as shown in Fig. 11.

Figure 12 depicts the variation of the Strouhal number as a function of Richardson number for different nanoparticles volume fractions. The ranges of Ri in which buoyancy has no effect on the Strouhal number are characterised by constant St-values. These ranges extend with increasing φ. compared to the results obtained in forced convection, when Ri reaches the value of 4.5, computations show that the Strouhal number has undergone an increase of 57%, 37% and 6% for $\varphi = 0\%$, $\varphi = 6\%$ and $\varphi = 12\%$ respectively.

The variation of the global time-averaged Nusselt number as a function of Ri at various φ is shown in Fig. 13. The ranges of Ri in which buoyancy has no effect on the heat transfer are characterized by constant $\langle \overline{Nu_t} \rangle$-values. As it is already observed in Fig. 10, the influence of buoyancy forces becomes more important beyond $Ri = 0.8$. All the curves

$\varphi = 0\%$ $\varphi = 12\%$

$(a): Ri = 0$

$(b): Ri = 1$

$(c): Ri = 3$

$(d): Ri = 4.5$
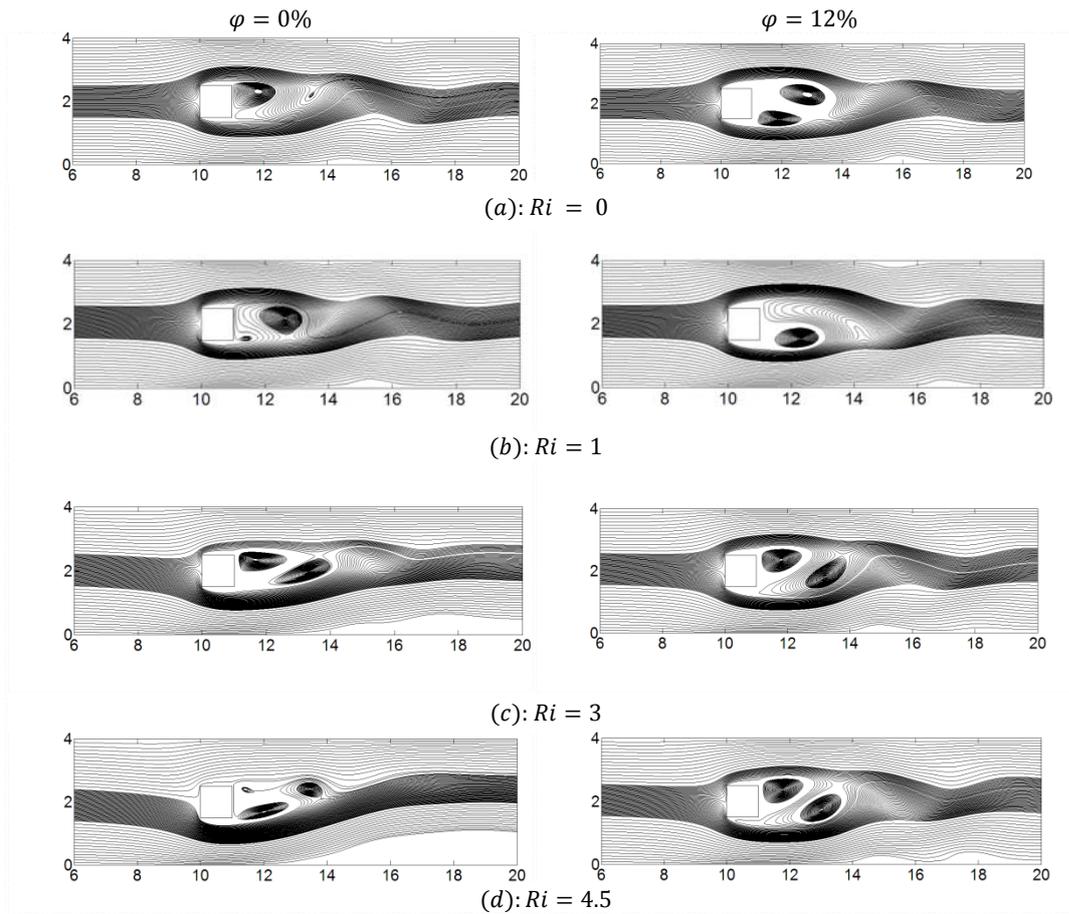
Fig. 9. Streamlines crossing the square cylinder in the channel for different Richardson numbers ($Re = 150$).
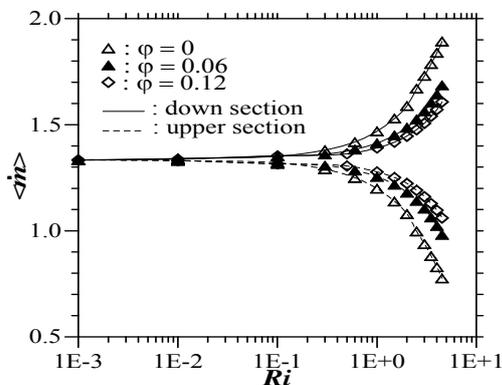
Fig. 10. Variation of the time-averaged flow rate vs Ri through the sections between the square cylinder and the channel walls for different φ ($Re = 150$).

Fig. 11. Evolution of the flow rate with time through the sections between the square cylinder and the channel walls ($Re = 150$ and $Ri = 2$).

show a remarkable increase beyond this value and tend towards an asymptotic value. Thus, the rate of the heat transfer increases significantly for $Ri > 0.8$.

Figure 14 depicts the variation of the global time-averaged Nusselt number versus φ for different Richardson numbers. As it can be seen, $\langle \overline{Nu_t} \rangle$ increases monotonously by increasing φ for all Richardson numbers and increases as the Richardson number increases for a fixed value of φ.

Indeed, the flow of Cu-water nanofluid becomes more intense, by increasing Ri and further improves the heat transfer. For each value of Richardson number and in a range of φ under consideration, numerical results show that $\langle \overline{Nu_t} \rangle$ varies linearly with respect to φ. Using the least-square method for all the computed values, the following expression may be derived:

For $i = 0$: $\langle \overline{Nu_t} \rangle = 10.684\,\varphi + 5.640$

$$(17\text{-}1)$$

1498

For $i = 1$: $\langle \overline{Nu_t} \rangle = 11.432 \, \varphi + 5.960$

(17-2)

For Ri = 4.5 : $\langle \overline{Nu_t} \rangle = 11.804 \, \varphi + 7.008$

(17-3)

These correlations have a maximum deviation of about 1% from the computed values.
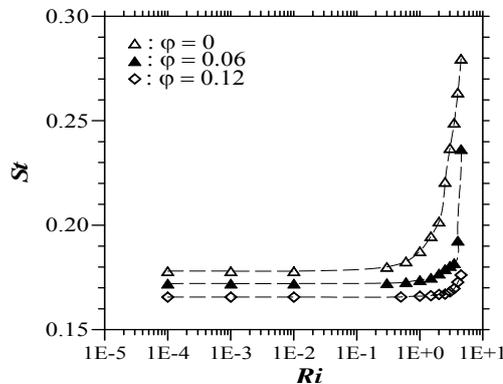
Fig. 12. Variation of St vs Ri for different $Re = 150$).
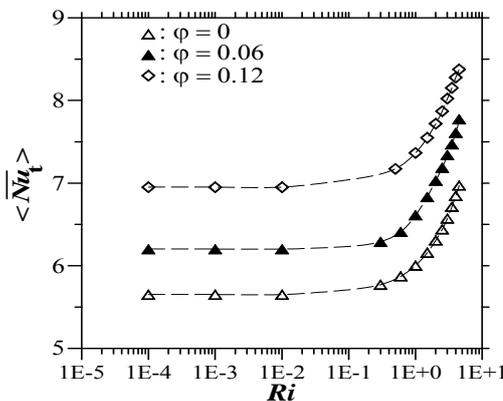
Fig. 13. Variation of $\langle \overline{Nu_t} \rangle$ vs Ri for different φ ($Re = 150$).
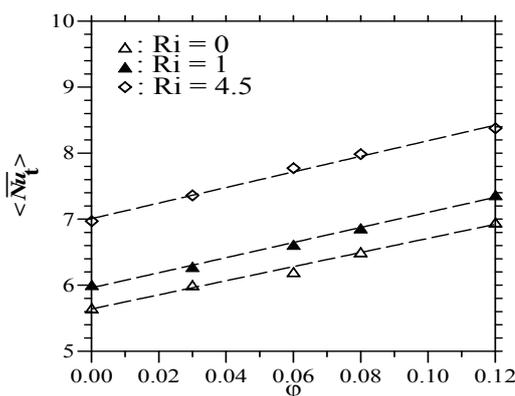
Fig. 14. Effect of Richardson number Ri on variation of $\langle \overline{Nu_t} \rangle$ with volume fraction φ.

5. CONCLUSIONS

A numerical investigation of unsteady, laminar and incompressible 2D flow and heat transfer of Cu-water nanofluid past a heated square cylinder inside horizontal channel was carried out. For $85 \leq Re \leq 200$ and $0 \leq \varphi \leq 12\%$, the following conclusions can be drawn:

In forced convection:

▪ The critical value of Reynolds number relative to transition from steady to periodic flow decreases rapidly by increasing the volume fraction, reaches a local minimum at $\varphi = 6\%$, after that it increases slightly as φ increases.

▪ At a fixed Reynolds number, the Strouhal number decreases by increasing the volume fraction.

▪ The presence of nanoparticles has a significant effect on the amplitude of oscillation of the lift coefficient which shows a significant increase by increasing the nanoparticles volume fraction, leading to unstable posture of the cylinder to the flow at higher Reynolds number.

▪ The global time-averaged Nusselt number $\langle \overline{Nu_t} \rangle$ over the heat transfer surface of the square cylinder can be correlated by the following relationships:

$$\langle \overline{Nu_t} \rangle = c \, Re^d$$

Values of the coefficient "c" and the exponent "d" are given by equations (16-1)-(16-3)

In mixed convection:

▪ For each nanoparticles volume fraction under consideration, the thermal buoyancy becomes significant when Ri exceeds 0.8. The heat transfer shows a remarkable increase compared to the one obtained in pure forced convection.

▪ For different Richardson numbers, The global time-averaged Nusselt number $\langle \overline{Nu_t} \rangle$ varies linearly with respect to the nanoparticles volume fraction. Correlations are given by equation (17-1)-(17-3)

REFERENCES

Abbassi, H, S. Turki and S. Ben Nasrallah (2002). Channel flow bluff-body: outlet boundary condition, vortex shedding and effects of buoyancy. *Computational Mechanics* 28, 10-16.

Bouaziz, M., S. Kessentini and S. Turki (2010). Numerical prediction of flow and heat transfer of power-law fluids in a plane channel with a built in heated square cylinder. *Int. J. Heat and Mass Transfer* 53, 5420-5429

Bouazizi, L., A. Ben Moussa and S. Turki (2013). Prediction of low Reynolds number flow over a square cylinder with a porous layer. *International Journal of Mechanic Systems Engineering* 3 (2), 83-88.

Breuer, M., J. Bernsdorf, T. Zeiser and F. Durst (2000). Accurate computations of the laminar flow past square cylinder based on two different methods: lattice-Boltzman and finite volume. *Int. J. Heat Fluid Flow* 21, 186–196.

Brinkman, H. C., (1952). The viscosity of concentrated suspensions and solutions. *J. Chem. Phys.* 20, 571–581

Darekar, R. M. and S. J. Sherwin (2001). Flow past a square-section cylinder with a wavy stagnation face. *J.Fluid Mech.* 426, 263-295

Daungthongsuk, W. and S. Wongwises (2007). A critical review of convective heat transfer of nanofluids. *Renew. Sustain. Energy Rev.* 11, 797–817.

Davis, R. W. and E. F. Moore (1982). A numerical study of vortex shedding from rectangles. *J. Fluid Mech.* 116, 475-506.

Fazeli, S. A., S. M. H. Hashemi, H. Zirakzadeh and M. Ashjaee (2012). Experimental and numerical investigation of heat transfer in a miniature heat sink utilizing silica nanofluid. *Superlattices and Microstructures* 51(2), 247-264.

Hashemi, S. M. H, S. A. Fazeli, H. Zirakzadeh and M. Ashjaee (2012). Study of heat transfer enhancement in a nanofluid-cooled miniature heat sink-volume average technique. *International Communications in Heat and Mass Transfer* 39(6), 877-884.

Kakaç, S. and A. Pramuanjaroenkij (2009). Review of convective heat transfer enhancement with nanofluids. *International Journal of Heat and Mass Transfer* 52, 3187-3196.

Kelkar, K. M. and S. V. Patankar (1992). Numerical prediction of vortex shedding behind a square cylinder. *Int. J. Numer. Methods Fluids* 14, 327–341.

Khanafer, K., K. Vafai and M. *Lightstone* (2003). Buoyancy-driven heat transfer enhancement in a two-dimensional enclosure utilizing nanofluids. *Int. J. Heat Mass Transfer* 46, 3639–3653.

Liu, Z. (2010). Square Cylinder Large Eddy Simulation Based on Random Inlet Boundary Condition. *Journal of Applied Fluid Mechanics* 3 (1), 35-45.

Mahian, O., A. Kianifar, S. A. Kalogirou, I. Pop and S. Wongwistes (2013). A review of the applications of nanofluids in solar energy. *International Journal of Heat and Mass Transfer* 57, 582–594.

Nayak, R. K., S. Bhattacharyya and I. Pop (2015). Numerical study on mixed convection and entropy generation of Cu–water nanofluid in a differentially heated skewed enclosure. *International Journal of Heat and Mass Transfer* 85, 620–634.

Patankar, S.V. (1980). Numerical heat transfer and fluid flow.*Series in Comp. Meth. In Mech. and Therm. Sc., Mac Graw hill.*

Rashad, A. M., A. J. Chamkha and M. M. M. Abdou (2013). Mixed Convection Flow of Non-Newtonian Fluid from Vertical Surface Saturated in a Porous Medium Filled with a Nanofluid. *Journal of Applied Fluid Mechanics* 6(2), 301-309.

Safaei, M. R., H. Togun, K. Vafai, S. N. Kazi and A. Badarudin (2014). Investigation of Heat Transfer Enhancement in a Forward-Facing Contracting Channel Using FMWCNT Nanofluids. *Numerical Heat Transfer, Part A: Applications* 66(12), 1321-1340.

Saidur, R., K. Y. Leong and H. A. Mohammad (2011). A review on applications and challenges of nanofluids. *Renew. Sustain. Energy Rev.* 15, 1646–1668.

Sarafraz, M. M., S. M. Peyghambarzadeh, F. Hormozi and N. Vaeli (2014). Experimental studies on the upward convective boiling flow to DI-water and CuO nanofluids inside the annulus. *Journal of Applied Fluid Mechanics* (09).

Sarkar, S., S. Ganguly and G. Biswas (2012). Mixed convective heat transfer of nanofluids past a circular cylinder in cross flow in unsteady regime. *Int. J. Heat Mass Transfer* 55, 4783–4799.

Sarkar, S., S. Ganguly and A. Dalal (2013). Buoyancy driven flow and heat transfer of nanofluids past a square cylinder in vertically upward flow. *Int. J. Heat Mass Transfer* 59, 433–450.

Sohankar, A., C. Norberg and L. Davidson (1998). Low-Reynolds number flow around a square cylinder at incidence: study of blockage, onset of vortex shedding and outlet boundary condition. *Int. J. Numer. Methods Fluids* 26, 39–56.

Sohel, M. R., R. Saidur, M. F. M. Sabri, M. Kamalisarvestani, M. M. Elias and A. Ijam (2013). Investigating the heat transfer performance and thermo physical properties of nanofluids in a circular micro-channel. *International Communications in Heat and Mass Transfer* 42, 75-81.

Turki, S. and G. Lauriat (1990a). Thermal convection of non-newtonian fluids in enclosures, *AIAA/ASME, Thermophysics and Heat Transfer Conference* 165-170.

Turki, S. and G. Lauriat (1990b). An examination of two numerical procedures for natural convection in composite enclosures, *AIAA/ASME Thermophys. Heat Transfert Conf. ASME-HTD* 130, 107-113.

Turki, S., H. Abbassi and S. Ben Nasrallah (2003). Effect of the blockage ratio on the flow in a channel with a built-in square cylinder. *Comput. Mech.* 33, 22–29.

Turki, S., H. Abbassi and S. Ben Nasrallah (2003). Two-dimensional laminar fluid flow and heat transfer in a channel with a built-in heated square cylinder, *Int. J. Therm. Sci.* 42, 1105–1113.

Valipoor, M. S., R. Masoodi, S. Rashidi, M. Bovand and M. Mirhosseini (2014). A numerical study on convectionaround a square cylinder using $AL_2O_3 - H_2O$ nanofluid.

Thermal science 18(4), 1305-1314.

Valipour, M. S. and A. Z. Ghadi (2011). Numerical investigation of fluid flow and heat transfer around a solid circular cylinder utilizing nanofluid, *Int. Comm. Heat Mass Transfer* 38, 1296–1304.

Xuan, Y. and Q. Li (2003). Investigation on convective heat transfer and flow features of nanofluids. *J. Heat Transfer* 125, 151–155.

Zirakzadeh, H., A. Mashayekh, H. N. Bidgoli and M. Ashjaee (2012). Experimental investigation of heat transfer in a novel heat sink by means of alumina nanofl uids. *Heat Transfer Research* 43(8), 709-720.